Acta Oceanol. Sin., 2015, Vol. 34, No. 11, P. 32–37
DOI: 10.1007/s13131-015-0745-1
http://www.hyxb.org.cn
E-mail: hyxbe@263.net

Modeling the interaction of an internal solitary wave with a sill

LI Qun[1], XU Zhenhua[2, 3*], YIN Baoshu[2, 3], BAI Tao[4], LIU Kun[2, 3, 5], WANG Yang[2, 3, 5]

[1] Polar Research Institute of China, Shanghai 200136, China

[2] Institute of Oceanology, Chinese Academy of Sciences, Qingdao 266071, China

[3] Key Laboratory of Ocean Circulation and Waves (KLOCAW), Chinese Academy of Sciences, Qingdao 266071, China

[4] North China Sea Marine Forecasting Center of State Oceanic Administration, Qingdao 266033, China

[5] University of Chinese Academy of Sciences, Beijing 100049, China

Received 19 March 2015; accepted 14 June 2015

Abstract

A nonhydrostatic numerical model was developed and numerical experiments performed on the interaction of an internal solitary wave (ISW) with a sill, for a two-layer fluid with a diffusive interface. Based on the blocking parameter (B_r), the flow was classified into three cases: (1) when bottom topography has little influence on the propagation and spatial structure of the ISW (B_r<0.5), (2) where the ISW is distorted significantly by the blocking effect of the topography (though no wave breaking occurs, (0.5<B_r<0.7), and (3) where the ISW is broken as it encounters and passes over the bottom topography (0.7<B_r). The numerical results obtained here are consistent with those obtained in laboratory experiments. The breaking process of the incident ISW when B_r≈0.7 was completely reproduced. Dissipation rate was linearly related to the blocking parameter when B_r<0.7, and the maximum dissipation rate could reach about 34% as B_r raised to about 1.0. After that, instead of breaking, more reflection happened. Similarly, breaking induced mixing was also most effective during B_r around 1.0, and can be up to 0.16.

Key words: internal solitary wave, nonhydrostatic model, wave breaking, blocking degree

Citation: Li Qun, Xu Zhenhua, Yin Baoshu, Bai Tao, Liu Kun, Wang Yang. 2015. Modeling the interaction of an internal solitary wave with a sill. Acta Oceanologica Sinica, 34(11): 32–37, doi: 10.1007/s13131-015-0745-1

1 Introduction

Numerous in situ and remote sensing observations have demonstrated evidence of packets of internal solitary waves (ISWs) in marginal seas, straits, fjords, and coastal waters (Osborne and Burch, 1980; Apel et al., 1985; Liu et al., 1998; Zhao and Alford, 2006; Zheng et al., 2007; Xu et al., 2010, 2011) Such waves may evolve from disturbances caused by tidal flow over topography (e.g., continental shelf breaks, oceanic banks, sills, and ridges) and probably constitute an important part of the energy transfer mechanism from large to smaller scales (Munk and Wunsch, 1998; Zhao et al., 2010). They contribute to vertical mixing while propagating at the interface where a shear layer develops. Shoreward-propagating waves eventually break in a coastal zone where they are thought responsible for nutrient mixing (Sandstrom and Elliot, 1984).

The present paper considers the propagation of an ISW in a two-layer fluid with a diffusive interface, which is a case that is particularly relevant to oceanic environments. The shoaling of such waves over uniformly sloping bottom topography has already been investigated experimentally (Helfrich and Melville, 1986; Michallet and Ivey, 1999; Chen et al., 2007) and numerically (Vlasenko and Hutter, 2002; Graham et al., 2009) because of the importance of this process in determining vertical mixing, sediment transport, and morphological changes at the seabed and on the continental shelf. However, only a few investigations have been conducted into the behavior of ISWs encountering isolated, two-dimensional bottom topography, i.e., the configuration under consideration here.

Wessels and Hutter (1996) conducted laboratory experiments on the passage of small amplitude internal waves of elevation over a bottom sill in a two-layer fluid with a sharp interface and they made careful measurements of the distortion caused to the waveform by the encounter. Further laboratory experiments by Hütteman and Hutter (Hütteman and Hutter, 2001) on ISWs of elevation passing over a sill considered the effects of the diffusive (stratified) interface separating the upper and lower homogeneous layers of a two-layer system. Their results revealed that the finite thickness of the interface is associated with the generation of higher order baroclinic modes, which were not found in previous experiments with a sharp interface. Sveen et al. (Sveen et al., 2002) performed laboratory experiments on the breaking properties of large amplitude ISWs of depression over a bottom ridge and the wave-induced currents were observed using a PIV (Particle Image Velocimetry) system. Specifically, the results were compared with a newly developed fully nonlinear ISW theory for a two-layer fluid (Grue et al., 2000). This theory, however, cannot describe the breaking properties, which are of particular interest when considering the energy cascade within the ocean. Furthermore, the properties of dissipation of a wave propagating through wave tank have been investigated. Based on a similar ex-

Foundation item: The National Natural Science Foundation of China under contract Nos 41528601 and 41376029; the Youth Innovation Promotion Association of Chinese Academy of Sciences under contract No. Y4KY07103L, the Strategic Priority Research Program of the Chinese Academy of Sciences under contract No. XDA11020101.

*Corresponding author, E-mail: xuzhenhua@qdio.ac.cn

perimental configuration, Guo et al. (2005) studied the flow structure of the interaction of an ISW with a bottom ridge. Kuo et al. (2005) conducted laboratory experiments on the interaction of ISWs with a sill, paying particular attention to the properties of the reflected and transmitted waves, and the statistical characteristics of the dissipation rate for differing blocking parameters were presented. Preliminary consideration of the mixing efficiency was also mentioned. Chen (2007) further studied the mixing process of a stratified flow during the interaction of an ISW with bottom ridge topography. He stated that the degree of blocking (Blocking parameter) could be applied to classify various degrees of ISW-obstacle encounter within a two-layer stratified fluid system. However, the primary difficulty regarding the above experiment is the calculation of the wave energy because of the lack of accurate measurement techniques and therefore, some approximation theory was employed (Helfrich, 1992; Grue et al., 2000).

The motivation for this study was the experimental results of Kuo (2005), Sveen et al. (2002), and Chen (2007). For comparison with their laboratory experimental results, a nonhydrostatic numerical model was developed and applied in this study, and the obtained simulated dissipation and mixing properties are considered here.

The remainder of this paper is organized as follows. Section 2 introduces the numerical model and configuration of the experiments. Typical experimental results are presented and analyzed in Section 3. The statistical properties of dissipation and mixing are provided and a quantitative comparison with available laboratory data presented in Section 4. Finally, the conclusions are offered in Section 5.

2 Governing equations and model setup

2.1 *Numerical equations*

A nonlinear, 2D nonhydrostatic numerical model with continuous vertical stratification and turbulent exchange was developed based on the stream function-vorticity equation. The 2D Cartesian x-z coordinate system was used, in which the x-axis represented the undisturbed free surface and the z-axis represented the vertical opposite to the direction of gravity. The system of equations describing the dynamics of a continuously stratified fluid can be written as:

$$\begin{aligned}
&\omega_t + J(\omega,\psi) = g\frac{\rho_x}{\rho_a} + a_h\omega_{xx} + a_v\omega_{zz},\\
&\rho_t + J(\rho,\psi) + \frac{\rho_a}{g}N^2(z)\psi_x = k_h\rho_{xx} + k_v[\rho+\rho_0(z)]_{zz},\\
&\omega = \psi_{xx} + \psi_{zz},\\
&u = \psi_z, w = -\psi_x,
\end{aligned} \tag{1}$$

where ψ is the 2D streamfunction, ω is vorticity, u and w are velocities, ρ, ρ_a, $\rho_0(z)$ are the wave-induced perturbations of the density, average density, and undisturbed density profiles, respectively, a_h and a_v are the horizontal and vertical coefficients of turbulent viscosity, respectively, k_h and k_v are the horizontal and vertical coefficients of density diffusion, respectively, $N(z)$ is the Brunt–Väisälä frequency, and $J(A,B) = \frac{\partial A}{\partial x}\frac{\partial B}{\partial z} - \frac{\partial A}{\partial z}\frac{\partial B}{\partial x}$ is the Jacobian operator.

In modeling the interaction of an ISW with topography, only the baroclinic motion of the ocean was considered. Thus, the model assumed a rigid-lid approximation and zero tangential wind stress on the free surface at $z = 0$. Therefore, on the free surface $z = 0$ we had:

$$\psi = 0, \omega = 0, \rho_z = 0. \tag{2}$$

The boundary condition for the density field implied the absence of heat and salt fluxes through the ocean surface. The conditions for the streamfunction and vorticity implied the absence of vertical motion and vertical shear of currents at the upper rigid-lid surface.

For the viscid case at the bottom $z = H(x)$, the kinematic no-slip condition and the absence of heat and salt fluxes were assumed:

$$\psi = 0, \psi_z = 0, \psi_x = 0, \rho_n = 0, \tag{3}$$

where n is the normal to the bottom.

The boundary value of vorticity ω at the bottom was estimated using the equation $\omega = \nabla^2\psi$, where the stream function ψ was taken from the previous temporal step.

The model equations with boundary conditions were numerically integrated using an alternative direction implicit scheme, and the Poisson equation for the stream function solved using a successive over relaxation iteration with Chebyshev acceleration. In practical applications for ISW simulations, the turbulent dissipation/diffusion coefficients should be maintained as small as possible. In our experiments values of $a_h = 1\times10^{-4}$ and $a_v = 1\times10^{-5}$ were used for the vorticity equation and values of $k_h = 1\times10^{-5}$ and $k_v = 1\times10^{-6}$ used for the diffusion coefficient. This choice of parameters allowed the ISW to propagate to tens of wavelengths without significant dissipation. For the difference grid, the values of $\Delta x = 2$ m and $\Delta z = 1$ m with a time step of $\Delta t = 1$ s were found stable for all experiments, including those where breaking occurred.

2.2 *Model configuration*

Initially, the water elevation and the velocities were zero. The background density distribution in the model was calculated according to:

$$\rho(z) = \rho_m + \frac{\Delta\rho}{2}\left[1 - \tanh\left(\frac{z+z_0}{\Delta h}\right)\right], \tag{4}$$

where, for a two-layer condition with an upper layer with density ρ_1 and a lower layer with density ρ_2, the parameters in the initial density profile can be written as $\rho_m = (\rho_1+\rho_2)/2$, $\Delta\rho = (\rho_2-\rho_1)$, z_0 is the interface depth, and Δh is the diffusive layer thickness. This density profile presents a two-layer system with a diffusive interface of thickness Δh. An example configuration and the generated incident wave are plotted in Fig. 1, in which $z_0 = 35$ m and $\Delta h = 3.5$ m. In our experiments, the topography was kept unchanged for incident ISWs with differing amplitudes and two pycnocline depths were considered, i.e., $z_0 = 15$ m, 35 m.

3 Model results and analysis

To understand the properties of the incident depression ISWs interacting with different sill parameters, a non-dimensional parameter is defined, i.e., the blocking degree (B_r), where $B_r = (a + h_1)/(h_1 + h_2 - h_r)$. When $B_r = 1$, the trough of the incident wave is just at the top of the sill. The sill has greater influence on the incident wave with bigger values of the blocking parameter. This definition of the blocking degree differs from that of Wessels and Hutter, (1996), in which it is defined as h_r/h_2, i.e., the ratio of the

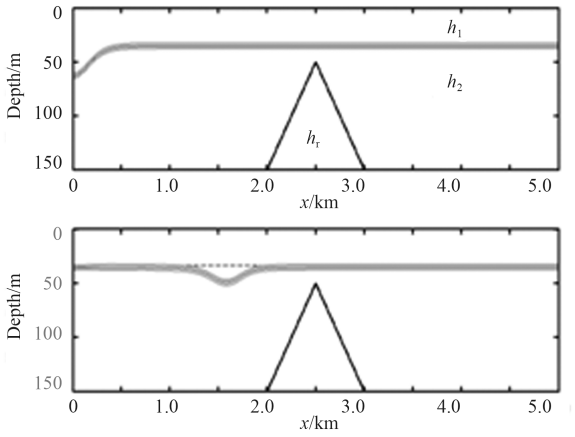

Fig. 1. Model configuration and generation of the incident internal solitary wave.

topography height to the lower-layer depth. In our experiments, the primary consideration was the properties of the ISWs of differing amplitudes interacting with the same topographic sill and therefore, the definition of the blocking degree given here is more reasonable. Furthermore, this definition is consistent with that of Kuo (2005) and thus, the direct comparison of our findings with their results is possible.

During the simulation with a shallow pycnocline (z_0 = 15), the blocking degree defined above lies in the range 0.35–0.7. When B_r < 0.5, the interaction is weak and the topography almost has no effect on the incident wave. As the wave passes over the ridge, the velocity in the lower layer is increased because of the reduced local depth, but no breaking occurs and the wave shape is not distorted significantly. As the relative blocking effect (0.5 < B_r < 0.7) exerted by the ridge is increased, the deformation of the wave changes from weak to moderate. The velocity in the lower layer is increased significantly because of the reduced local water depth. Separation is observed to take place at the ridge, but no significant breaking/mixing is observed after the encounter. In most cases, separation leads to the generation of one or more vortices that propagate along the bottom and eventually dissipate near the top of the ridge. The thickness of the interface is increased after the passage of the incident wave, but no mixing or overturning occurs as the wave passes over the ridge. These results are similar to the laboratory experiments.

When B_r > 0.7 (calculations for a deep pycnocline, i.e., z_0 = 35 m) strong breaking occurs. Figure 2 illustrates successive instances in the process of a depression ISW over an isolated ridge in the numerical experiment with B_r = 1.08 (wave propagates from left to right), during which wave breaking can be observed. The profile of the incident ISW is deformed as it approaches the leading face of the triangular ridge (Figs 2a and b). The front of the leading wave is aligned almost parallel to the slope. Three minutes later, as shown in Fig. 2c, the leading wave exhibits its steepest profile during its strong downward motion along the leading face of the ridge. The pycnocline becomes thicker than its original condition on the leading face of the ridge (Fig. 2d), in which the top layer is thicker than the bottom layer. An internal hydraulic jump is illustrated between Figs 2c and d, where signs of vortex mixing can be seen at the lowest point of the interface. The incident depression-type ISW with a sech² shape then transforms into a triangular waveform, and this transformation is followed by strong upward motion that produces an elevated internal bore (Figs 2b–f). This process resembles a depression-type ISW running up sloping topography (Michallet and Ivey, 1999). In Figs 2c–f, the stratified interface at the lowest point shows signs of diffusion due to mixing between the fluids of the upper and lower layers. The mixing of the lower layer high density water with the upper layer low density water creates a fog-like diffusion on the stratified interface, inducing flow intrusion because of the breaking wave energy. The wave profile overturns in a clockwise direction Figs 2c–f) and the front of the internal bore becomes obscured by the blending of the upper layer water (Figs 2e and f). The velocity field corresponding to Fig. 2e is shown in Fig. 3. It can be seen that during this breaking process, several strong vortices are generated (also called bolus in several other papers (Helfrich and Melville, 1986; Michallet and Ivey, 1999)) and these strong vortices have significant implications regarding the vertical mixing and bottom boundary-layer processes.

These results demonstrate that the ISW eventually broke and fluid mixing occurred at certain intervals when an isolated ridge was encountered. Stratified fluid mixing is a commonly observed feature of internal waves. Here, the internal bore becomes so sharp that the pycnocline overturns/collapses locally, as shown in Figs 2c–f. Wave collapse is nonlinear and it is extremely difficult to describe analytically or numerically using a simplified long-wave model (Hütteman and Hutter, 2001). A simple heuristic description of the main physical mechanism is that it involves

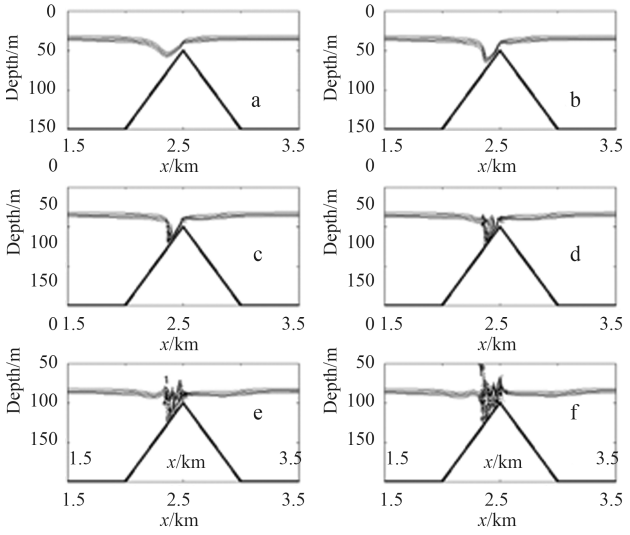

Fig. 2. A typical interaction process where breaking occurs (time interval between panels is 1.5 min).

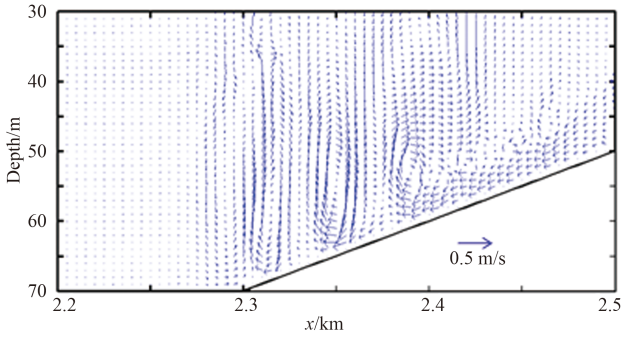

Fig. 3. Velocity field corresponding to the density field in Fig. 2e.

a hydraulic jump, i.e., a rapid, nearly instantaneous jump in the water depth. The formation of a depression-type waveform with a triangular structure draws upper layer water downward to promote hydraulic jumps on the leading face of the apex of the submarine ridge (Fig. 2c). Internal hydraulic jumps cause fluid mixing in a stratified two-layer fluid system. However, hydraulic jumps followed by a vortex inside the lower fluid body did not occur here, i.e., significant breaking and mixing during weak or moderate wave–obstacle encounters. An elevated internal bore behind the leading pulse could also be considered as a transition of the critical flow occurring between the wave trough and the leading face of an isolated ridge. Local downward flow is critical for strong interaction between an ISW and a submerged ridge (i.e., Figs 2c–f). The internal hydraulic jump shown between Figs 2c and d eventually transforms into a rising perturbation bolus on the initial interface (Figs 2e and f), which could be deduced from the velocity field in Fig. 3. Additionally, these internal bores can have amplitudes as high as the initial leading wave. The internal bores eventually disintegrated into trains of internal waves while propagating over the submarine ridge.

4 Energy dissipation and mixing efficiency

4.1 *Energy dissipation rate*

When an ISW propagates over a submarine obstacle, the energy of the incident ISW is dissipated, for example, by shoaling, reflection, transmission, and breaking. From this, the energy dissipation rate E_p can be defined as:

$$E_{diss} = E_i - E_r - E_t, \tag{5}$$

$$E_p = E_{diss}/E_i \times 100\#, \tag{6}$$

where E_i is the incident wave energy, E_r is the energy of the reflected wave, and E_t is the energy of the transmitted wave.

In the numerical experiments, the calculation of the wave energy (Gill, 1982) was more accurate than in the laboratory experiments (Kuo, 2005), in which only the leading wave energy was considered and the estimation was based on linear two-layer theory (Helfrich, 1992). The wave energy was calculated as a time integral of the depth-integrated energy flux F at the base of the sill (two sides for the calculation of the transmitted and reflected wave energy), i.e.:

$$E_i = \int_{t_0}^{t_1} F\mathrm{d}t, E_r = \left|\int_{t_2}^{t_3} F\mathrm{d}t\right| \text{ and } E_t = \int_{t_4}^{t_5} F\mathrm{d}t, \tag{7}$$

where the time intervals were chosen visually to include the entire wave period. The depth-integrated energy flux was calculated as:

$$F = \int_H^0 u\left[p' + \rho_0\left(u^2 + w^2\right)/2\right]\mathrm{d}z, \tag{8}$$

where p' is the wave-induced pressure (i.e., the instantaneous pressure minus the pressure in the undisturbed state), and u and w represent the horizontal and vertical velocity components, respectively.

Energy dissipation rate versus the blocking degree is plotted in Fig. 4. It can be seen that the energy dissipation rate is proportional to the blocking degree. The dissipation rate increases together with B_r. When $B_r < 0.5$, the energy dissipation rate is no more than 15%, and in this case, the friction dissipation of the wave energy might be the primary factor. As B_r increases further, more significant energy dissipation is presented, especially in the breaking case; the maximum the dissipation rate can reach is about 34%. Compared with the results of the laboratory experiments, the general trend of energy dissipation is consistent. However, as B_r increases, a discrepancy become clearer, i.e., the energy dissipation rate in the numerical calculation is smaller than that of Kuo (2005). This could be attributed partially to the method of estimating the wave energy. As only the energy of the leading wave was considered, this might underestimate the wave energy, especially when wave breaking occurred (bigger B_r) and some secondary smaller waves were generated. These small amplitude waves could be reflected or transmitted. Another factor that should be considered is strong frictional dissipation in the laboratory experiments, which has been mentioned by Wessels and Hutter (1996). In our numerical calculations, experiments with strong horizontal dissipation coefficients were performed and the results are plotted in Fig. 4. From these calculation results, it can be deduced that the comparatively high dissipation rate of Kuo (2005) could be attributed to the method of estimation and the strong frictional dissipation in the laboratory experiments.

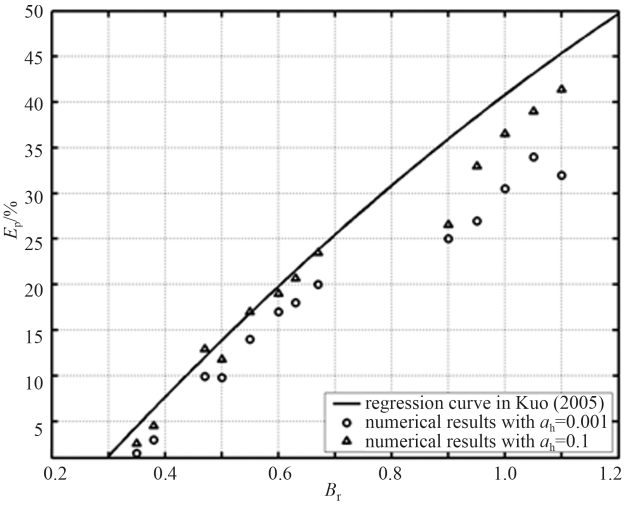

Fig. 4. Comparison of the modeled dissipation rate and laboratory results (dissipation rate E_p versus blocking degree B_r)

4.2 *Mixing efficiency*

During a wave–sill encounter, continual mixing in the breaking zone leads to a slow diffusion of the mean density gradient in the stratified fluids. The amount of mixing can be estimated by the changes in the vertical profiles of density before and after an experiment. Mixing efficiency, defined as the ratio of the increase of potential energy and the amount of wave energy lost on the slope, has been reported for several test cases on different normal slopes (Ivey and Nokes, 1989; Slinn and Riley, 1996).

These authors defined mixing efficiency R_f as:

$$R_f = \Delta PE / \left[E_i - (E_r r + E_t t)\right], \tag{9}$$

where ΔPE is the difference in potential energy before and after the interaction. Mixing efficiency R_f versus the blocking parameter B_r is plotted in Fig. 5, together with a least-squares fitted curve. Within the range of our considered parameters, the mixing effi-

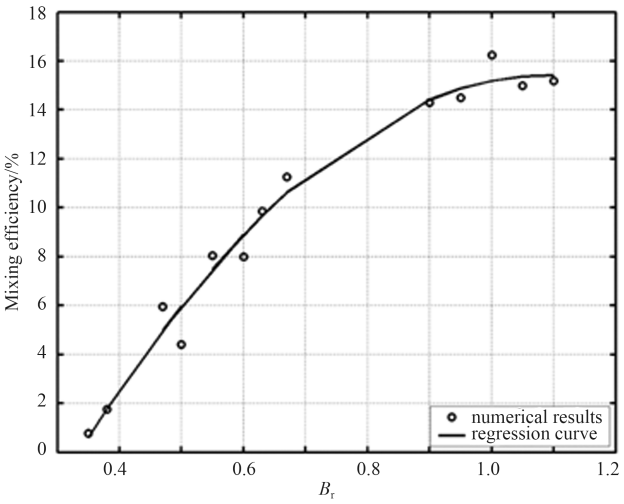

Fig. 5. Mixing efficiency with different blocking parameters (solid line: regression curve, f=–26.9x^2+58.7x–16.7).

ciency grows as the blocking parameter increases. The general trend is in accord with the dissipation rate. However, there are no available laboratory data for comparison (probably because of the difficulties in measuring the relative variables). In fact, as the blocking parameter increases further, especially beyond $h_r > h_2$, a decrease in the dissipation rate can be found (Vlasenko and Hutter, 2002). This is because more wave energy is reflected but no breaking occurs over the topography and therefore, a corresponding decrease in the mixing efficiency can be expected.

The calculation results of mixing efficiency, however, are only for the purpose of illustrating the mixing properties during the interaction of an ISW with a submerged sill topography in the numerical calculation. Because of the limitations of our numerical model, some sub-grid turbulent mixing process, which play important roles in stratified flow mixing, cannot be modeled directly. Therefore, the calculation here might underestimate the mixing efficiency, as indicated by Helfrich, (1992) in the laboratory experiments. For a thorough understanding of the mixing process in a stratified fluid, fine-resolution numerical modeling and a turbulent closure model will be necessary.

5 Conclusions

Weakly nonlinear theory has been widely used for the study of ISW. It can successfully reproduce the propagation and disintegration of ISW over variable topography and compared well with satellite and in situ observations (Yuan et al., 2006; Zheng et al., 2015). However, as highly simplified theoretical equation, it cannot be used to study the breaking and mixing process of ISW. In this case, it is more suitable to use the direct numerical simulations to investigate the structure and energetic of breaking internal waves over variable topography.

The presented modeling results showed the propagating properties of an ISW in a stratified two-layer fluid system and the consequences of an encounter between such a wave and a 2D bottom ridge. The primary consequences have been shown to be the transient generation of vortices within the stratified fluid, for cases where the amplitude of the incident wave and ridge height are both relatively large ($0.7 < B_r$). For such cases, the overturning motions in the upper layer are associated directly with the wave breaking over the ridge; a process that produces significant turbulent mixing within the layer and across the interfacial region between the upper and lower layers. The vigor of the turbulent mixing and resulting thickness of the pycnocline were found to be determined by the amplitude of the incident wave and height of the ridge; findings that are consistent with the results of previous studies (Sveen et al., 2002; Guo et al., 2005; Kuo, 2005; Chen, 2007). However, many other factors affect the interaction process. The estimations of the mixing efficiency and dissipation rate were approximate. The main purpose in performing the numerical calculations was comparison with available laboratory experimental Data. Therefore, in this study, several critical nondimensional parameters were kept constant and consistent with those of the laboratory experiments, and only the variation of the incident wave amplitude was considered. In fact, experiments with topography of different length scales have shown that the slope of the sill also has significant influence on the interaction process. In particular, when breaking occurs and a strong vortex structure is generated, the intensity of the vortex formation is dependent both on the amplitude of the wave and on the wavelength of the bottom topography, with the effect of the latter being shown to be surprisingly strong.

References

Apel J R, Holbrook J R , Liu A K , et al. 1985. The Sulu Sea internal soliton experiment. J Phys Oceanogr, 15(12): 1625–1651

Chen Chenyuan. 2007. An experimental study of stratified mixing caused by internal solitary waves in a two-layered fluid system over variable seabed topography. Ocean Engineering, 34(14–15): 1995–2008

Chen Chenyuan, Hsu J R-C, Chen H-H, et al. 2007. Laboratory observations on internal solitary wave evolution on steep and inverse uniform slopes. Ocean Engineering, 34(1): 157–170

Gill A E. 1982. Atmosphere–Ocean Dynamics. New York: Academic Press, 138–142

Grue J, Jensen A, Rusås P-O, et al. 2000. Breaking and broadening of internal solitary waves. J Fluid Mech, 413: 181–217

Guo Yakun, Sveen J K, Davies P A, et al. 2005. Modelling the motion of an internal solitary wave over a bottom ridge in a stratified fluid. Environmental Fluid Mechanics, 4(4): 415–441

Helfrich K R. 1992. Internal solitary wave breaking and run-up on a uniform slope. J Fluid Mech, 243: 133–154

Helfrich K R, Melville W K. 1986. On long nonlinear internal waves over slope-shelf topography. J Fluid Mech, 167: 285–308

Hüttemann H, Hutter K. 2001. Baroclinic solitary water in a two-layer fluid system with diffusive interface. Exp Fluids, 30(3): 317–326

Ivey G N, Nokes R I. 1989. Vertical mixing due to the breaking of critical internal waves on sloping boundaries. J Fluid Mech, 204: 479–500

Kuo C F. 2005. Experimental study on the evolution and effect of bottom obstacle on internal solitary wave[dissertation]. Taiwan: National Sun Yat-Sen University

Liu A K, Chang Y S, Hsu M-K, et al. 1998. Evolution of nonlinear internal waves in the East and South China Seas. J Geophys Res, 103(C4): 7995–8008, doi: 10.1029/97JC01918

Michallet H, Ivey G N. 1999. Experiments on mixing due to internal solitary waves breaking on uniform slopes. J Geophys Res, 104(C6): 13467–13477

Munk W, Wunsch C. 1998. Abyssal recipes II: energetics of tidal and wind mixing. Deep-Sea Res Pt I, 45(12): 1977–2010

Osborne A R, Burch T L. 1980. Internal solitons in the Andaman Sea. Science, 208(4443): 451–460

Rickard G, O'Cllaghan J, Popinet S. 2009. Numerical simulations of internal solitary waves interacting with uniform slopes using an adaptive model. Ocean Modelling, 30(1): 16–28

Sandstrom H, Elliot J A. 1984. Internal tide and solitons on the Scotian Shelf: A nutrient pump at work. J Geophys Res, 89(C4): 6415–6426

Slinn D N, Riley J J. 1996. Turbulent mixing in the oceanic boundary layer caused by internal wave reflection from sloping terrain.

Dynamics of Atmospheres and Oceans, 24(1–4): 51–62
Sveen J K, Guo Yakun, Davies P A, et al. 2002. On the breaking of internal solitary waves at a ridge. J Fluid Mech, 469: 161–188
Vlasenko V I, Hutter K. 2002. Numerical experiments on the breaking of solitary internal waves over a slope-shelf topography. J Phys Oceanogr, 32(6): 1779–1793
Wessels F, Hutter K. 1996. Interaction of internal waves with a topographic sill in a two-layered fluid. J Phys Oceanogr, 26(1): 5–20
Xu Zhenhua, Yin Baoshu, Hou Yijun, et al. 2010. A study of internal solitary waves observed on the continental shelf in the northwestern South China Sea. Acta Oceanol Sin, 29: 18–25
Xu Zhenhua, Yin Baoshu, Hou Yijun. 2010. Highly nonlinear internal solitary waves over the continental shelf of the northwestern South China Sea. Chin J Oceanol Limonol, 28(5): 1049–1054
Xu Zhenhua, Yin Baoshu, Hou Yijun. 2011. Response of internal solitary waves to tropical storm Washi in the northwestern South China Sea. Ann Geophys, 29: 2181–2187, doi: 10.5194/angeo-29-2181-2011
Yuan Yeli, Zheng Quan'an, Dai Dejun, et al. 2006. Mechanism of internal waves in the Luzon Strait. J Geophys Res, 111(C11): C11S17, doi: 10.1029/2005JC003198
Zhao Zhongxiang, Alford M H. 2006. Source and propagation of internal solitary waves in the northeastern South China Sea. J Geophys Res, 111(C11): C11012, doi: 10.1029/2006JC003644
Zhao Zhongxiang, Alford M H, MacKinnon J A, et al. 2010. Long-range propagation of the semidiurnal internal tide from the Hawaiian Ridge. J Phys Oceanogr, 40(4): 713–736, doi: 10.1175/2009JPO4207.1
Zheng Quan'an, Susanto R D, Ho C-R, et al. 2007. Statistical and dynamical analyses of generation mechanisms of solitary internal waves in the northern South China Sea. J Geophys Res, 112(C3): C03021, doi: 10.1029/2006JC003551
Zheng Quan'an, Zhu Benlu, Li Junyi, et al. 2015. Growth and dissipation of typhoon-forced solitary continental shelf waves in the northern South China Sea. Climate Dyn, 45(3): 853–865, doi: 10.1007/s00382-014-2318-y